Opto-Electronic Advances

Special Issue for Xiamen University Centenary Celebration

Original Article

2021, Vol. 4, No. 4

DOI: 10.29026/oea.2021.200061

Laser direct writing and characterizations of flexible piezoresistive sensors with microstructures

Chenying Zhang[1], Wei Zhou[1]*, Da Geng[1], Cheng Bai[1], Weida Li[1,2], Songyue Chen[1]*, Tao Luo[1], Lifeng Qin[1] and Yu Xie[1]

Functional materials with high viscosity and solid materials have received more and more attentions in flexible pressure sensors, which are inadequate in the most used molding method. Herein, laser direct writing (LDW) method is proposed to fabricate flexible piezoresistive sensors with microstructures on PDMS/ MWCNTs composites with an 8% MWCNTs mass fraction. By controlling laser energy, microstructures with different geometries can be obtained, which significantly impacts the performances of the sensors. Subsequently, curved microcones with excellent performance are fabricated under parameters of f = 40 kHz and v = 150 mm·s^{-1}. The sensor exhibits continuous multi-linear sensitivity, ultrahigh original sensitivity of 21.80 % kPa^{-1}, wide detection range of over 20 kPa, response/recovery time of ~100 ms and good cycle stability for more than 1000 times. Besides, obvious resistance variation can be observed when tiny pressure (a peanut of 30 Pa) is applied. Finally, the flexible piezoresistive sensor can be applied for LED brightness controlling, pulse detection and voice recognition.

Keywords: flexible pressure sensor; piezoresistive sensor; microstructure; laser processing

Zhang CY, Zhou W, Geng D, Bai C, Li WD et al. Laser direct writing and characterizations of flexible piezoresistive sensors with microstructures. *Opto-Electron Adv* **4**, 200061 (2021).

Introduction

With the development of flexible electronics, biomedical tests, intelligent robots, internet of things and so on, flexible pressure sensors have received extensive attention due to the important roles played in signal acquisition and conversion[1–15]. According to responding signals, flexible pressure sensors can be divided into piezoresistive sensors[3–6], capacitive sensors[7–9], piezoelectric sensors[10,11] and triboelectric sensors[12,13]. Among these flexible pressure sensors, flexible piezoresistive sensors have advantages including simple structures, high sensitivity, short response time, and so on[6,16,17]. Besides, continuous emerging of advanced materials including metallic nanowires[5,18–20], carbon nanotubes[2,3,21,22], graphene[6,23–25] and MXenes[4,26,27] benefits the performances of piezoresistive sensors. Consequently, flexible piezoresistive sensors with excellent performances have been increasingly investigated.

It has been reported that the performances of flexible piezoresistive sensors can be remarkably improved by introducing microstructures on substrates[6,17,21,23,28–32]. Up to now, the molding method has been regarded as the most

[1]Department of Mechanical & Electrical Engineering, Xiamen University, Xiamen 361101, China; [2]College of Information Science and Engineering, Northeastern University, Shenyang 110004, China..

*Correspondence: W Zhou, E-mail: weizhou@xmu.edu.cn; SY Chen, E-mail: s.chen@xmu.edu.cn

Received: 30 September 2020; Accepted: 26 November 2020; Published online: 6 April 2021

efficient and widely-used method for fabricating flexible sensors with microstructures. For example, Park et al.[21] fabricated an electronic skin (E-skin) with microstructures by patterning the composites of polydimethylsiloxane (PDMS) and multiwall carbon nanotubes (MWCNTs) with etched silicon molds. Bae et al.[23] fabricated a PDMS piezoresistive sensor with hierarchical microstructures using an etched and thermal oxidized copper mold. Inspired by skin epidermis microstructures, Pang et al.[28] developed a piezoresistive sensor by molding PDMS with abrasive papers and subsequently coating with reduced graphene oxide (rGO). Nie et al.[29] fabricated a piezoresistive E-skin with hierarchical mountain-ridges microstructures by patterning PDMS on a banana leave. However, the molding method is mainly limited to the formation of microstructures for materials with relatively low viscosity (e.g. pure PDMS), which is inadequate for solid materials (e.g. MXenes and porous graphene) and materials with high viscosity (e.g. composites of CNTs at a high mass fraction).

In this paper, a laser direct writing (LDW) method was proposed to fabricate flexible piezoresistive sensors with microstructures using a PDMS/MWCNTs composite (MPC) of an 8% MWCNTs mass fraction. Laser processing has advantages including high fabrication efficiency, low processing cost and high dimensional resolution[33–37]. Subsequently, surface geometry of microstructures can be adjusted by controlling laser energy, which significantly influenced the performances of flexible piezoresistive sensors. When laser parameters were set to be f = 40 kHz and v = 150 mm·s^{-1}, curved cone-like microstructures can be obtained. This sensor showed ultrahigh sensitivity (21.80 % kPa^{-1}), wide detection range (over 20 kPa), short response/recovery time (~100 ms), high resolution (a peanut for 30 Pa) and good cycle stability (1000 times). Finally, this sensor was applied in LED brightness controlling, pulse detection and voice recognition.

Materials and methods

Material preparation

MWCNTs were bought from Nanjing XFNANO Materials Tech. Co., Ltd. The specific parameters of the CVD MWCNTs were: external diameter of 10~20 nm, length of 10~30 μm, purity of more than 95%, tap density of 0.22 g/cm^3, true density of ~2.1 g/cm^3 and electrical conductivity of more than 100 S/cm. The morphology of MWCNTs was imaged by a field emission scanning electron microscope (FESEM) (SUPRA55 SAPPHIRE, Germany) and shown in Fig. S1(a) (see Supplymentary information). PDMS (SYLGARD 184) and the curing agent were supplied by Dow Corning Co. Ltd, USA. Firstly, PDMS was uniformly mixed with curing agent at a mass ratio of 10:1. Subsequently, MWCNTs were gradually added into PDMS under a continuous stirring to obtain uniform mixture of an 8% MWCNTs mass fraction. Next, the mixture was degassed for 10 minutes, uniformly coated on a 1 mm thick glass sheet and cured at 75 °C for 1 hour. Finally, the cured MPC was peeled off from the glass. The morphologies of PDMS and MPC were imaged by a scanning electron microscope (SEM) (JSM-IT500A, Japan), as shown in Figs. S1(b)–(c).

Mechanical characterizations

The mechanical properties including Youngs modulus and lateral contraction of both PDMS and MPC were evaluated by a tensile experiment. One end of a testing sample was fixed with a clamp and another end was stretched with a slider. The stretching force was measured by a force meter (Handpi HP-5N, China) and the size of the testing sample was measured by a digital vernier caliper. Detailed evaluations of mechanical properties are provided in Supplementary information S2.

Laser processing and morphology observation of microstructures

An ultraviolet (UV) laser marking machine (SEAL-355-10S, JPT, China) was employed for LDW of MPC. The basic parameters of the UV laser were shown in Table S1. The experimental parameters for LDW were shown in Table S2. The surface morphologies of microstructures were characterized by a SEM and a super deep scene 3D microscope (VHX5000, KEYENCE, Germany).

Design and assembly of flexible piezoresistive sensor

Flexible piezoresistive sensor consists of PI (polymide) tapes, interdigital electrodes and a MPC substrate, as shown in Fig. 1. Firstly, a Au film of 50 nm was deposited on a PET (polyethylene terephthalate) film of 50 μm using a magnetron sputtering apparatus (EXPLORER-14, USA). Secondly, the Au/PET film was patterned to fabricate interdigital electrodes by ablating the Au film using a UV laser marking machine. Then, the Au/PET film and MPC substrate were laser cut into certain size. Finally, Au/PET interdigital electrodes were assembled

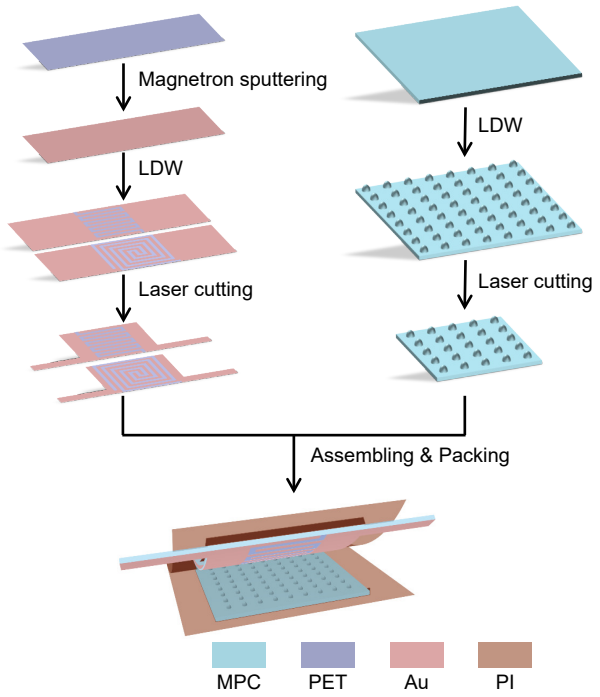

Fig. 1 | Design and fabrication of flexible piezoresistive sensor.

with the MPC substrate and packed with 50 μm thick PI tapes. Typical snake-like (SLI) and concentric-ring shape (CRI) separation areas were designed for fabricating interdigital electrodes.

Electrical characterizations

During the experiments, the sensor was fixed on a horizontal table. A pressure meter was employed to apply pressure to the top surface of the sensor. The electrical signals were measured by a digital source meter (Keithley 2400). When a pressure was applied, variation curves of the sensor including real-time resistance (*R*-*T*) and current-voltage (*I*-*V*) were acquired and recorded by computer. Besides, dynamic time resistance (*R*-*T*) curves were obtained to evaluate the response time and recovery time of the sensor.

Applications of flexible piezoresistive sensor

Flexible piezoresistive sensor was employed for LED brightness controlling, pulse detection and voice recognitions. For LED brightness controlling, the sensor was connected in series with an LED, and subsequently paralleled with a direct current power source of 12 V. For pulse detection, the sensor was fixed on the wrist of a tester to obtain resistance variation during pulse beats. For voice recognition, the sensor was attached on vocal cords of a tester to obtain resistance variation during speaking.

Results and discussion

Mechanical properties of materials

The thickness of PDMS and MPC decreased with the increasing ε_z, as shown in Fig. 2(a). Young's modulus of PDMS and MPC were evaluated by σ_z-ε_z curves, as shown in Fig. 2(b). Young's modulus of MPC was evaluated to be 3.31 MPa, which was higher than that of PDMS (0.95 MPa). It can be attributed to the higher mechanical stiffness of MWCNTs than that of PDMS[38]. Nevertheless, MPC still showed good flexibility for fabrication of flexible sensor.

Fabrication of microstructures

The LDW processing system of microstructures is shown in Fig. 3(a). A parallel laser scanning strategy (circles of 0.3 mm diameter, offsetting of 1 mm and line spacing of 0.05 mm) was proposed for LDW, as shown in Fig. 3(b). Microstructures were processed under 4 times of orthometric scanning. The schematic of laser processing is shown in Fig. 3(c). When a laser beam was focused on the surface of MPC, the exposed material was ablated due to photochemistry and photothermic effects.

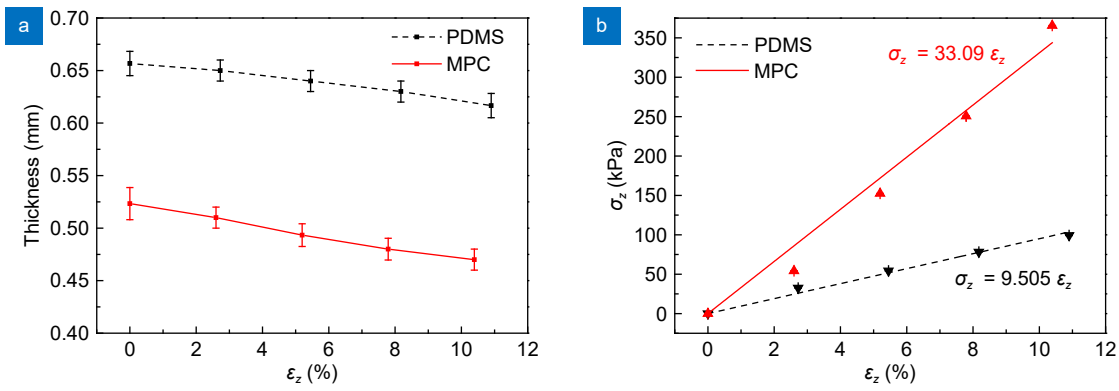

Fig. 2 | Mechanical properties of materials. (**a**) Lateral contraction of MPC and PDMS, (**b**) σ_z-ε_z curves of MPC and PDMS.

Notably, the ablation can be controlled by adapting parameters including laser repetition frequency f and scanning speed v. Variation of laser power and pulse with laser repetition frequency is shown in Fig. S3. When a low laser repetition frequency f and a fast scanning speed v was adopted, low microstructures were obtained due to a fairly low laser energy density[33,39], as shown in Fig. 3(d). With the increase of laser repetition frequency f, the laser power and pulse time were accordingly increased, and the laser spot was enlarged, thus increasing the ablation depth and ablation width. When laser scanning speed v was decreased, the ablation depth and ablation width were also increased due to higher energy density. The curved microstructures can be obtained due to the Gaussian distribution of laser energy[40], as shown in Fig. 3(e). When a higher laser repetition frequency f and a slower scanning speed v were adopted, a fairly high energy density was obtained, thus bringing about approximate

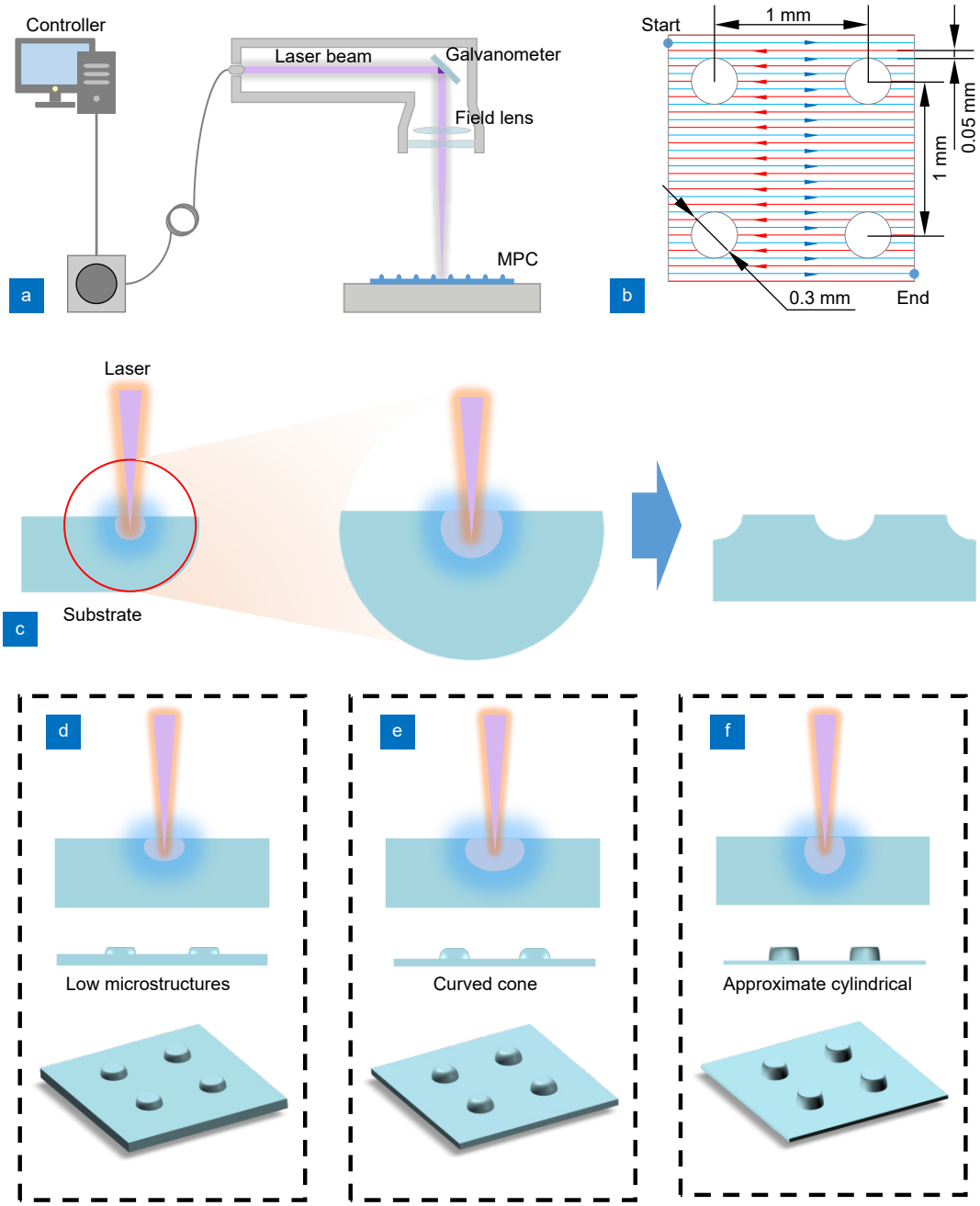

Fig. 3 | Fabrication of microstructures. (**a**) Processing system of LDW. (**b**) Laser scanning strategy. (**c**) Schematic of laser processing. (**d**) Processing schematic of low microstructures. (**e**) Processing schematic of curved cone-like microstructures. (**f**) Processing schematic of approximate cylindrical microstructures.

cylindrical microstructures with larger height, as shown in Fig. 3(f).

Surface morphology of microstructures

Surface morphologies of microstructures under different laser processing parameters were shown in Fig. 4 and Fig. S4. A lower laser repetition frequency or a faster scanning speed resulted in a lower material removal rate, so lower microstructures were observed, as shown in Figs. 4(c) and 4(f). Increasing the laser frequency or decreasing the scanning speed induced an elevated laser energy density, so curved cone-like microstructures were observed, as shown in Figs. 4(a), 4(b), 4(d), 4(e), 4(h) and 4(i). Application of a high laser frequency and a lower scanning speed resulted in an extremely high laser energy density, which caused destruction to microstructures. Therefore, approximate cylindrical microstructures with large height but poor surface were observed, as shown in Fig. 4(g). Besides, quantities of particles around microstructures were found, as shown in Figs. S4(g, h), which further demonstrated that the microstructures were seriously destroyed due to an excessive high laser energy density.

Performances of the flexible piezoresistive sensor

SLI and CRI interdigital electrodes were designed as Figs. 5(a)–5(b). Subsequently, the interdigital electrodes were fabricated by LDW and packed with MPC substrate by PI tapes, as shown in Figs. 5(c)–5(d). The interdigital electrodes were electrically connected by microstructures over the separation area. Near the separation area, electrical current flow along the path of interdigital electrode 1→ microstructure i→ substrate→ microstructure j→ interdigital electrode 2. The total resistance of the sensor R_{total} can be calculated as follow:

$$R_{\text{row}} = R_{\text{electrodes}} + R_{Ci} + R_{Vi} + R_{\text{substrate}} + R_{Cj} + R_{Vj} \quad , \tag{1}$$

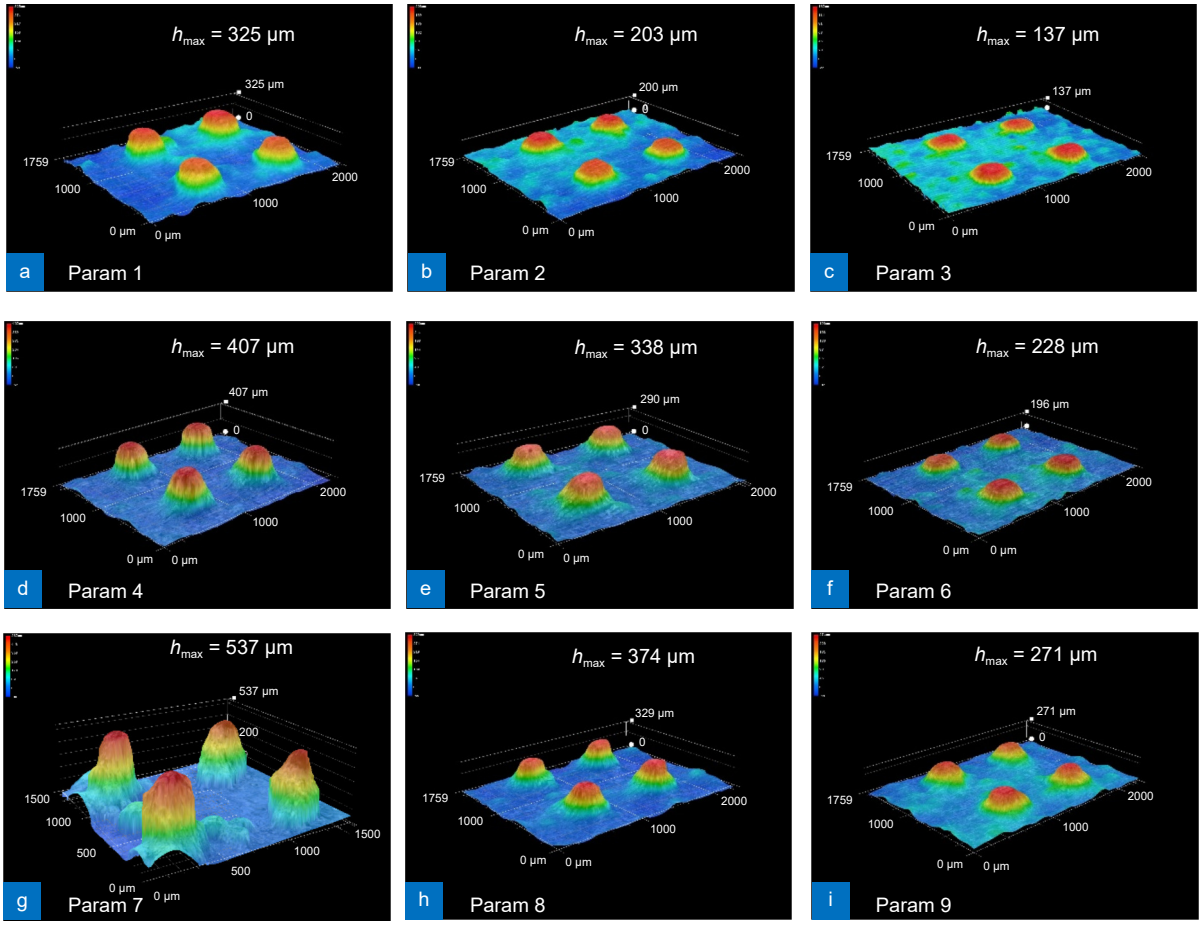

Fig. 4 | Surface morphologies of microstructures fabricated with different laser parameters imaged by a super deep scene 3D microscope. (**a**) **Param 1**: f = 35 kHz, v = 100 mm·s^{-1}; (**b**) **Param 2**: f = 35 kHz, v = 150 mm·s^{-1}; (**c**) **Param 3**: f = 35 kHz, v = 200 mm·s^{-1}; (**d**) **Param 4**: f = 40 kHz, v = 100 mm·s^{-1}; (**e**) **Param 5**: f = 40 kHz, v = 150 mm·s^{-1}; (**f**) **Param 6**: f = 40 kHz, v = 200 mm·s^{-1}; (**g**) **Param 7**: f = 45 kHz, v = 100 mm·s^{-1}; (**h**) **Param 8**: f = 45 kHz, v = 150 mm·s^{-1}; (**i**) **Param 9**: f = 45 kHz, v = 200 mm·s^{-1}.

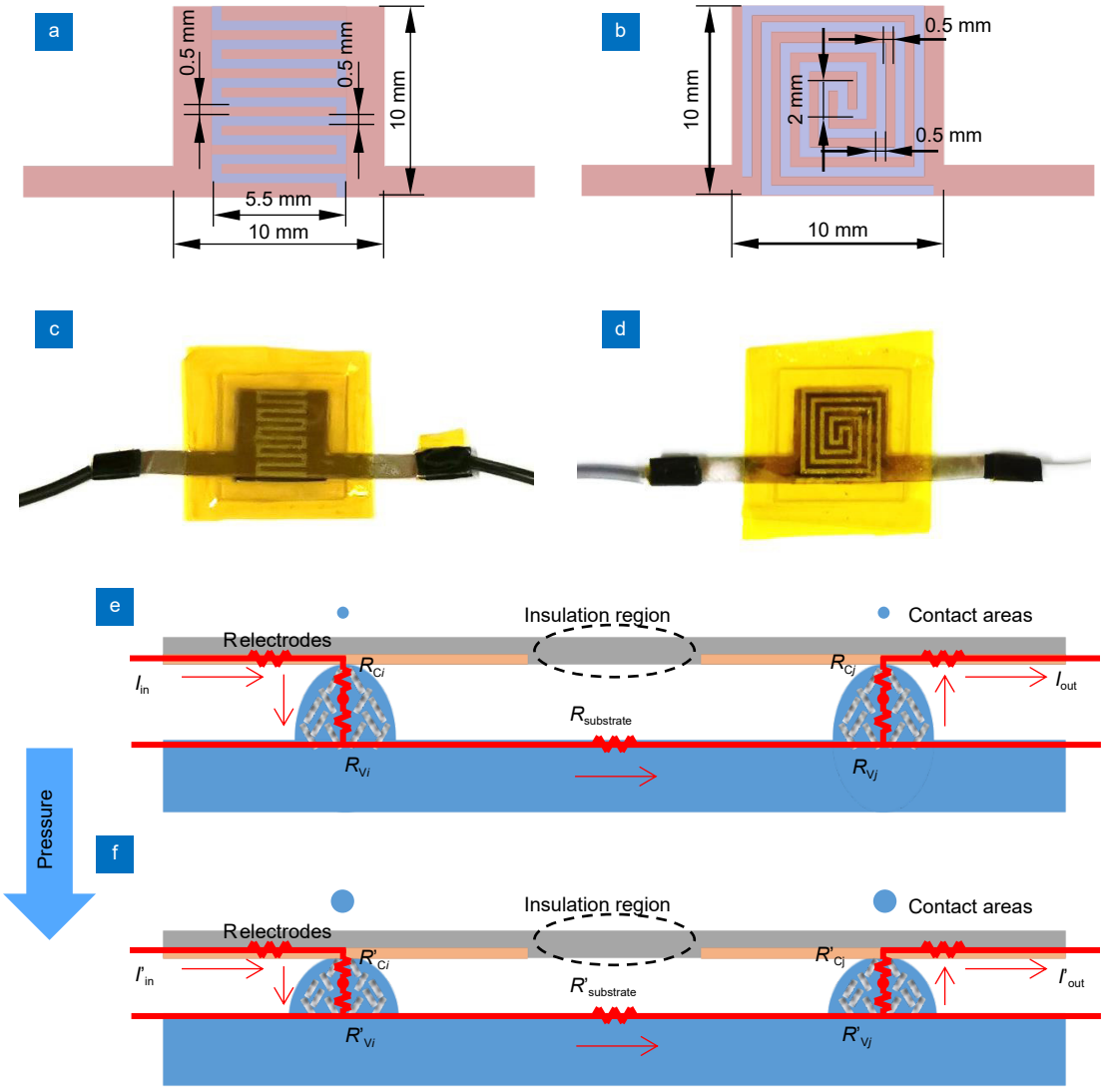

Fig. 5 | (**a**) Design of SLI interdigital electrodes. (**b**) Design of CRI interdigital electrodes. (**c**) Image of a sensor with SLI interdigital electrodes. (**d**) Image of a sensor with CRI interdigital electrodes. (**e**, **f**) Equivalent model of resistance in flexible piezoresistive sensors (e) without pressure, (f) under pressure.

$$R_{\text{total}} = \frac{1}{\frac{1}{R_{\text{row},1}} + \frac{1}{R_{\text{row},2}} + \cdots + \frac{1}{R_{\text{row},n}}}, \tag{2}$$

where $R_{\text{electrodes}}$ is the resistance of interdigital electrodes, R_{Ci} and R_{Cj} are the contact resistance between microstructures and interdigital electrodes, R_{Vi} and R_{Vj} are the volume resistance of microstructures, $R_{\text{substrate}}$ is the resistance of MPC substance, $R_{\text{row},\,k}$ (k = 1, 2, … , n) represents resistance of each row. Therein, $R_{\text{electrodes}}$ can be ignored due to the excellent conductivity of the gold interdigital electrodes. Thus the total resistance is mainly determined by volume resistance and contact resistance.

The equivalent resistance model of flexible piezoresistive sensors is shown in Figs. 5(e)–5(f). When a pressure was applied, the MPC substrate was deformed and the crosslink state of MWCNTs became closer[21], which decreasing R_{Vi}, R_{Vj} and $R_{\text{substrate}}$. Besides, the contact area between microstructures and interdigital electrodes was increased, thus significantly decreased R_{Ci} and R_{Cj}. As a result, R_{total} decreased with the increasing pressure applied. Further, sensitivity S of flexible piezoresistive sensors was defined as followed:

$$S = \frac{\mathrm{d}(\Delta R/R_0) \times 100\%}{\mathrm{d}(\Delta P)}, \tag{3}$$

where ΔP is the variation in pressure applied on the sensor, R_0 is the resistance of flexible piezoresistive sensor without pressure, and ΔR is the variation of sensor resistance. The units of ΔP, R_0 and ΔR are kPa, kΩ and kΩ, respectively.

Sensitivity properties of the sensors processed at

different laser parameters are shown as Fig. 6(a) and Fig. S5. When laser parameters were set to Param 7 (f = 45 kHz and v = 100 mm·s^{-1}), the sensor demonstrated low sensitivity, which can be attributed to the poor morphologies of the microstructures. When scanning speed was set to 150 mm·s^{-1} (Param 2, Param 5 and Param 8), sensors showed significantly higher sensitivity and wider detection range than the planar one. It can be concluded that the curved cone-like microstructures brought obvious variation in contact areas under pressure, and the deformation of microstructures increased with the increase of pressure. Especially, when laser processing parameters were set to Param 5 (f = 40 kHz and v = 150 mm·s^{-1}), the sensor exhibited the highest original sensitivity of 21.80 % kPa^{-1} and a wider detection range of over 20 kPa, which was employed for further experiments. The performance comparison between sensors with different designed interdigital electrodes was shown in Fig. 6(b). The original resistances of sensors with CRI and SLI interdigital electrodes were set through a precompression. The resistances of both sensors showed similar trends with ΔP. Namely, the shape of isolation areas in interdigital electrodes hardly affected the sensitivity of flexible piezoresistive sensors. In view of the processing efficiency of interdigital electrodes, SLI interdigital electrodes were adopted for further experiments. Properties of the sensors fabricated with Param 5 and packed with SLI interdigital electrodes were shown in Figs. 6(c) and 6(d). As shown in Fig. 6(c), this sensor showed obvious and multi-linear resistance variation with increasing pressure, which indicated good sensitivity. As shown in Fig. 6(d), this sensor showed linear I-V curves under different pressure, which indicated good resistance stability. When dynamic load was applied, the resistance response was shown in Fig. 7 and Video S1. Under stepped load, the sensor showed obvious resistance variation, as shown in Fig. 7(a). Besides, resistance variation can also be observed while tiny pressure (a peanut, ~30 Pa) was dropped, and response time and recovery time were ~100 ms, as shown in Fig. 7(b). Figure 7(c) showed the cycle stability of the sensor at 7 kPa, the resistance variation kept stable after 1000 cycle times.

Comprehensive comparisons between flexible-piezoresistive sensor in this work and references were shown in Fig. 8 and Table S3. In these references, sensitivities were also defined by Eq. (3), and these sensors showed either high original sensitivity but low detection range or wide detection range but low sensitivity.

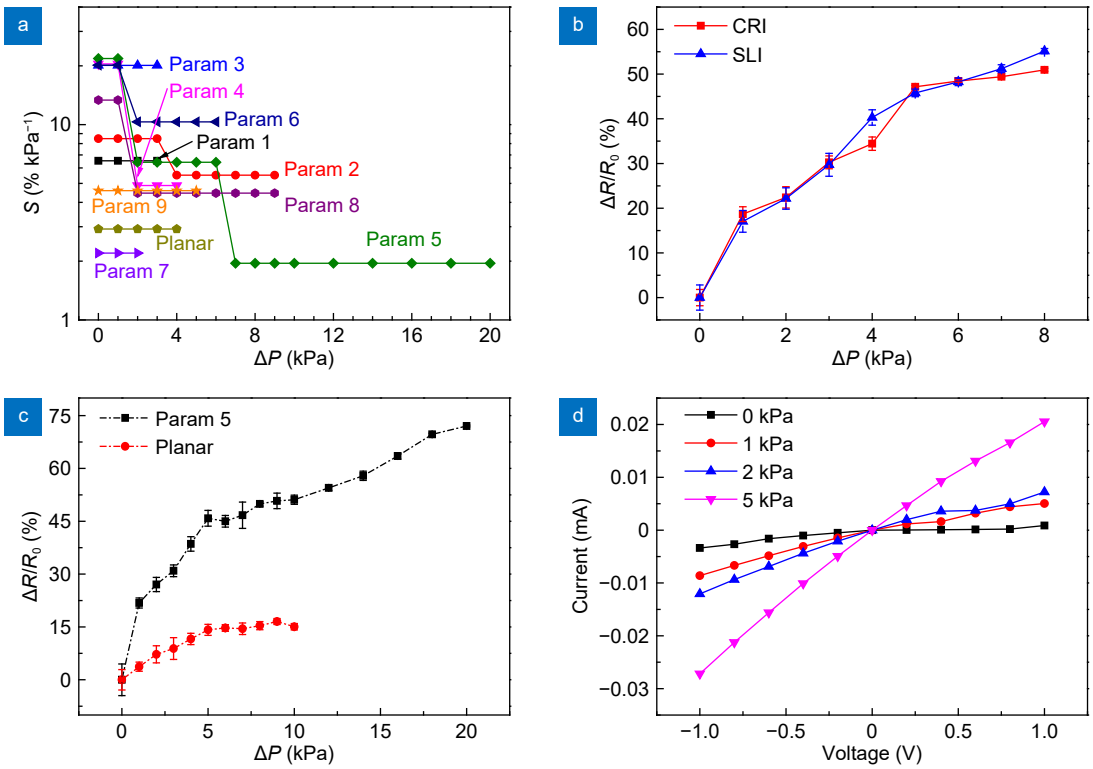

Fig. 6 | (**a**) Sensitivity properties of flexible piezoresistive sensors fabricated with different laser processing parameters. (**b**) Resistance variations with pressure of sensors packed with different interdigital electrodes within 8 kPa pressure. (**c**) Resistance variations with pressure of sensors fabricated with Param 5 and the planar one without microstructures. (**d**) I-V curves of sensor fabricated with Param 5 under different pressure.

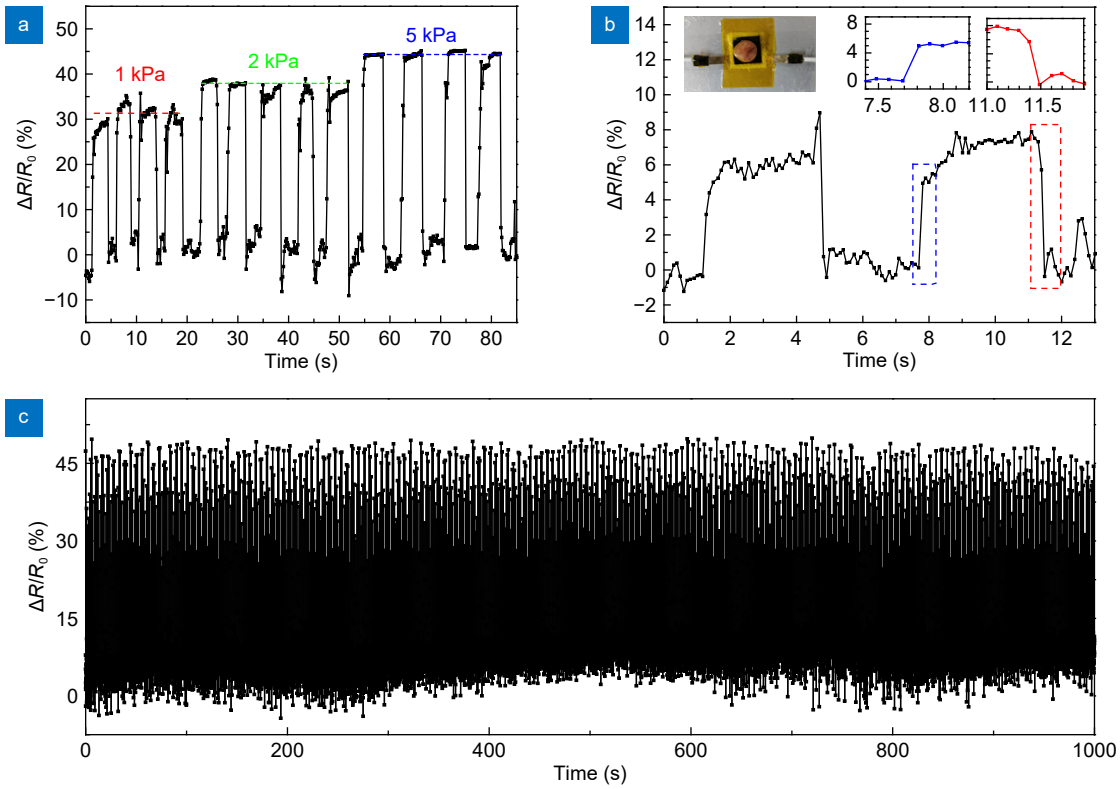

Fig. 7 | (**a**) Resistance variation toward step load. (**b**) Resistance variation toward pressure of a peanut. (**c**) Cycle stability within 1000 cycle times at 7 kPa pressure.

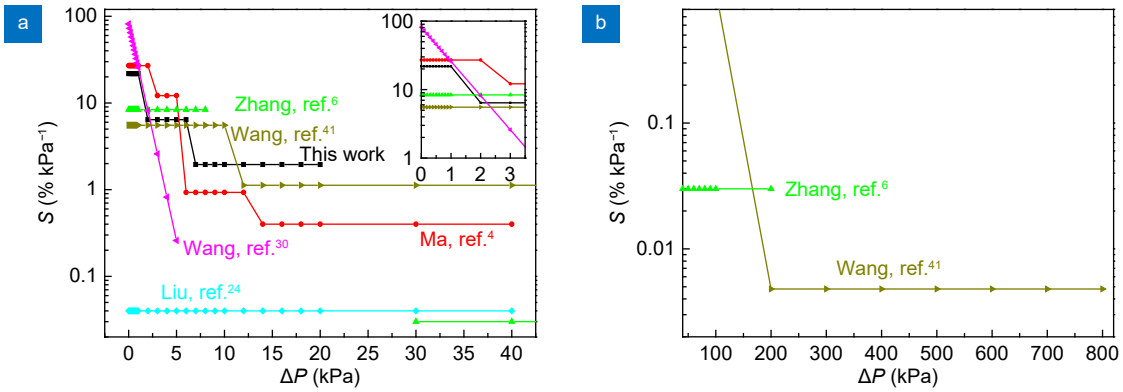

Fig. 8 | Sensitivity variations with pressure of this work and typical references[4,6,24,30,41]. (**a**) Within 40 kPa pressure. (**b**) Over 40 kPa pressure.

Moreover, some flexible piezoresistive sensor showed obvious nonlinear or discontinuous sensitivity within certain pressure range[6]. In comparison of references defining sensitivity by Eq. (3), the units were unified to be "% kPa^{-1}" and our sensors showed promised sensitivity properties (21.80, 6.42 and 1.95 % kPa^{-1} in range of 0~1, 1~5 and 5~20 kPa, continuous multi-linear) compared with references (ref.[4]: ~25, ~10, ~0.8 % kPa^{-1} and ~0.3 in the range of 0~2, 2~6, 6~10 and 10~35 kPa; ref.[6]: 8.36 and 0.028 % kPa^{-1} in the ranges of 0~8 and 30~200 kPa, but nonlinear from 8~30 kPa; ref.[23]: 0.04 % kPa^{-1} in the range of 0~40 kPa; ref.[30]: exponent damped sensitivity $y = 70.86\exp(-1.15x)$ in the range of 0~5 kPa; ref.[41]: 5.54, 0.123, 0.0048 % kPa^{-1} in the ranges of 0~10, 10~100 and 100~800 kPa). Besides, the proposed LDW method is simple, low cost and universal to a broad range of materials.

Applications of the flexible piezoresistive sensor

The sensor was applied for LED brightness controlling, pulse detection and voice recognition. In LED brightness controlling, as shown in Fig. 9(a) and Video S2, the initial resistance of sensors was high, so the series connected LED couldn't be lit up before pressing. The LED light up at pressing the sensor with a finger, as a result of

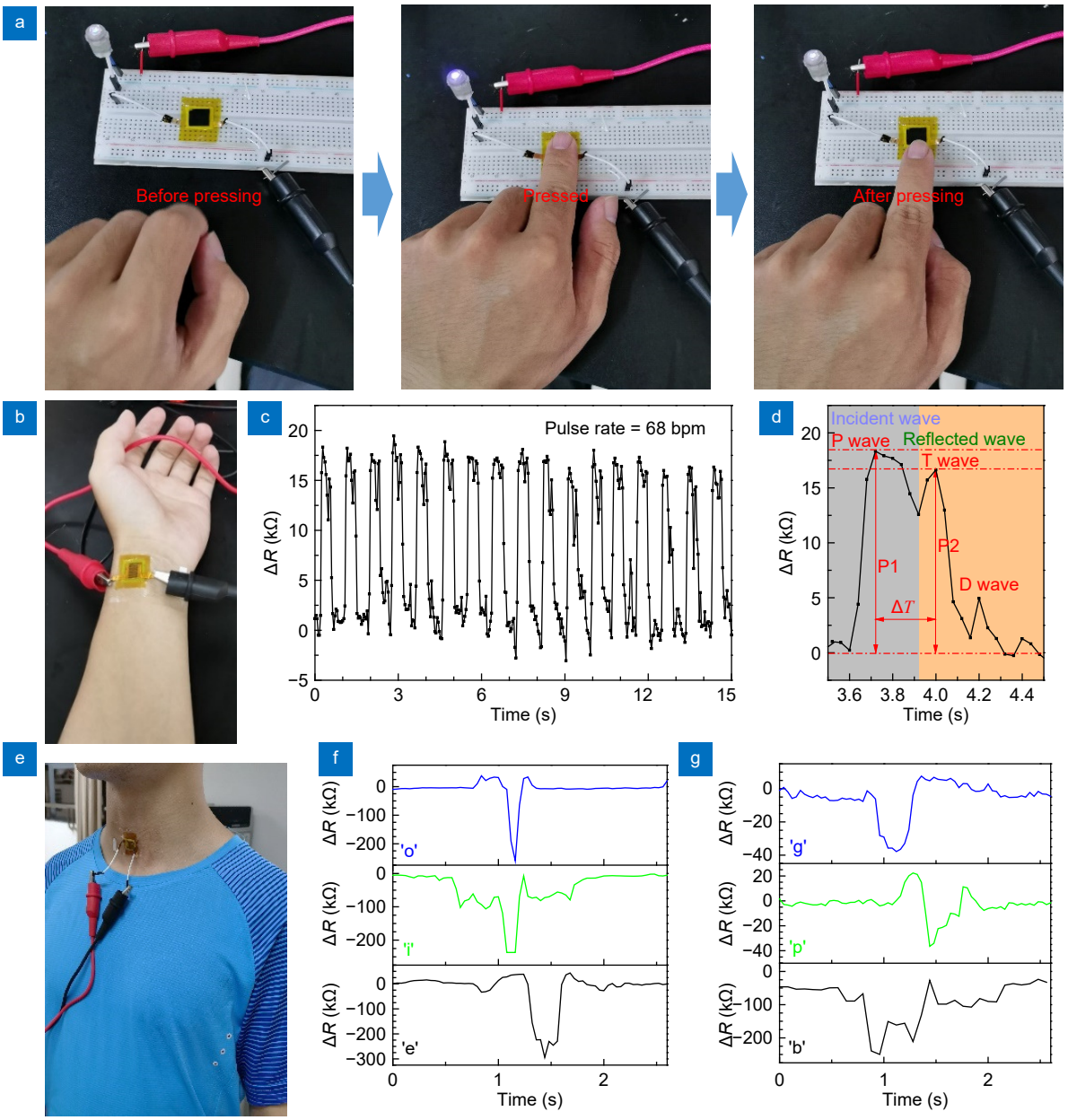

Fig. 9 | Applications of the flexible piezoresistive sensor. (**a**) LED brightness controlling. (**b**) Pulse detection. (**c**) Pulse wave detected from wrist. (**d**) Magnified wave from panel (c). (**e**) Voice recognition from vocal cords. (**f**) Waves of different vowels. (**g**) Waves of different consonants.

reduced sensor resistance. When the finger moved away, the resistance recovered and the LED turned dark again. As shown in Figs. 9(b)–9(d) and Video S3, a flexible piezoresistive sensor was attached on the wrist of a male tester of 24 years for detecting wrist pulse. During pulse beat, the resistance of the sensor decreased due to blood pressure on wrist surface, and the recorded wave and magnified signal were shown in Figs. 9(b) and 9(c). Three characteristic peaks called percussion wave (P-wave), tidal wave (T-wave), and diastolic wave (D-wave) can be observed, which indicates the incident wave from the heartbeat, reflected wave from the hands and reflected wave from the lower part of the body, respectively[42–45]. The peaks of P-wave and T-wave (P1 and P2) were respectively related to the systolic and diastolic blood pressure. The delay time ΔT between P1 and P2 was employed to estimate arterial stiffness. Herein, ΔT was estimated to be ~280 ms, which is consistent with literature data of a healthy male in his 20s[44]. The application of the sensor for voice recognition was shown in Figs. 9(e)–9(g) and Video S4. When the tester pronounced letters, resistance of the sensor attached to vocal cords changed with the shock energy. For a certain letter, resistance changes were consistent during test

several times, as shown in Video S4. For the different vowels, the resistance variations varied differently, both in tendencies and amplitudes.

Conclusions

LDW method was applied for the flexible piezoresistive sensor fabrication, with microstructures on PDMS/MWCNTs composites of an 8% MWCNTs mass fraction and interdigital electrodes on an Au/PET film. By controlling laser energy, microstructures with different geometries were obtained, which modulated the performances of flexible piezoresistive sensors. When laser processing parameters were set to f = 40 kHz and v = 150 mm·s^{-1}, the obtained curved microcones rendered the sensor continuous multi-linear sensitivity, with ultrahigh original sensitivity of 21.80 % kPa^{-1} and wide detection range of more than 20 kPa. The shape of the separation areas in interdigital electrodes hardly affected the sensitivity of the sensors. In dynamic responding, the sensors showed short response/recovery time of ~100 ms, high resolution to tiny pressure (a peanut of 30 Pa) and excellent cycle stability (1000 times). Therefore, the flexible piezoresistive sensor was applied in LED brightness controlling, pulse detection and voice recognition. Additionally, the LDW method exhibites advantages of simple process, high efficiency, low cost and general applicability for most materials. Our work provides a simple and versatile method for fabricating flexible piezoresistive sensors using solid materials (e.g. MXenes and porous graphene) or materials with high viscosity (e.g. composites of CNTs at a high mass fraction), where each part of the sensor including the microstructures and the interdigital electrodes can be efficiently fabricated without the mask.

References

1. Chen WF, Yan X. Progress in achieving high-performance piezoresistive and capacitive flexible pressure sensors: a review. *J Mater Sci Technol* **43**, 175–188 (2020).
2. Chun S, Son W, Choi C. Flexible pressure sensors using highly-oriented and free-standing carbon nanotube sheets. *Carbon* **139**, 586–592 (2018).
3. Deka BK, Hazarika A, Kim J, Jeong HE, Park YB et al. Fabrication of the piezoresistive sensor using the continuous laser-induced nanostructure growth for structural health monitoring. *Carbon* **152**, 376–387 (2019).
4. Ma YN, Liu NS, Li LY, Hu XK, Zou ZG et al. A highly flexible and sensitive piezoresistive sensor based on MXene with greatly changed interlayer distances. *Nat Commun* **8**, 1207 (2017).
5. Wei Y, Chen S, Dong XC, Lin Y, Liu L. Flexible piezoresistive sensors based on "dynamic bridging effect" of silver nanowires toward graphene. *Carbon* **113**, 395–403 (2017).
6. Zhang L, Li HQ, Lai XJ, Gao TY, Yang J et al. Thiolated Graphene@Polyester fabric-based multilayer piezoresistive pressure sensors for detecting human motion. *ACS Appl Mater Interfaces* **10**, 41784–41792 (2018).
7. Ma LQ, Yu XC, Yang YY, Hu YG, Zhang XY et al. Highly sensitive flexible capacitive pressure sensor with a broad linear response range and finite element analysis of micro-array electrode. *J Materiomics* **6**, 321–329 (2020).
8. Yang XF, Wang YS, Qing XL. A flexible capacitive sensor based on the electrospun PVDF nanofiber membrane with carbon nanotubes. *Sens Actuators A Phys* **299**, 111579 (2019).
9. Tay RY, Li HL, Lin JJ, Wang H, Lim JSK et al. Lightweight, superelastic boron nitride/polydimethylsiloxane foam as air dielectric substitute for multifunctional capacitive sensor applications. *Adv Funct Mater* **30**, 1909604 (2020).
10. Jeong SI, Lee EJ, Hong GR, Jo Y, Jung SM et al. Three-dimensional multistack-printed, self-powered flexible pressure sensor arrays: piezoelectric composites with chemically anchored heterogeneous interfaces. *ACS Omega* **5**, 1956–1965 (2020).
11. Xu MZ, Kang H, Guan L, Li HY, Zhang MN. Facile fabrication of a flexible $LiNbO_3$ piezoelectric sensor through hot pressing for biomechanical monitoring. *ACS Appl Mater Interfaces* **9**, 34687–34695 (2017).
12. Wang HL, Kuang SY, Li HY, Wang ZL, Zhu G. Large-area integrated triboelectric sensor array for wireless static and dynamic pressure detection and mapping. *Small* **16**, 1906352 (2020).
13. Fan FR, Lin L, Zhu G, Wu WZ, Zhang R et al. Transparent triboelectric nanogenerators and self-powered pressure sensors based on micropatterned plastic films. *Nano Lett* **12**, 3109–3114 (2012).
14. Yuan LQ, Wang ZW, Li HW, Huang YN, Wang SG et al. Synergistic resistance modulation toward ultrahighly sensitive piezoresistive pressure sensors. *Adv Mater Technol* **5**, 1901084 (2020).
15. Zhang T, Li ZY, Li K, Yang XN. Flexible pressure sensors with wide linearity range and high sensitivity based on selective laser sintering 3D printing. *Adv Mater Technol* **4**, 1900679 (2019).
16. Pang Y, Zhang KN, Yang Z, Jiang S, Ju ZY et al. Epidermis microstructure inspired graphene pressure sensor with random distributed spinosum for high sensitivity and large linearity. *ACS Nano* **12**, 2346–2354 (2018).
17. Yang CF, Li LL, Zhao JX, Wang JJ, Xie JX et al. Highly sensitive wearable pressure sensors based on three-scale nested wrinkling microstructures of polypyrrole films. *ACS Appl Mater Interfaces* **10**, 25811–25818 (2018).
18. Liao XQ, Zhang Z, Kang Z, Gao FF, Liao QL et al. Ultrasensitive and stretchable resistive strain sensors designed for wearable electronics. *Mater Horiz* **4**, 502–510 (2017).
19. Kaps S, Bhowmick S, Gröttrup J, Hrkac V, Stauffer D et al. Piezoresistive response of quasi-one-dimensional ZnO nanowires using an in situ electromechanical device. *ACS Omega* **2**, 2985–2993 (2017).
20. Cao MH, Wang MQ, Li L, Qiu HW, Padhiar MA et al. Wearable rGO-Ag NW@cotton fiber piezoresistive sensor based on

the fast charge transport channel provided by Ag nanowire. *Nano Energy* **50**, 528–535 (2018).
21. Park J, Kim J, Hong J, Lee H, Lee Y et al. Tailoring force sensitivity and selectivity by microstructure engineering of multidirectional electronic skins. *NPG Asia Mater* **10**, 163 –176 (2018).
22. Zhang ZM, Zhang YX, Jiang X, Bukhari H, Zhang ZX et al. Simple and efficient pressure sensor based on PDMS wrapped CNT arrays. *Carbon* **155**, 71–76 (2019).
23. Bae GY, Pak SW, Kim D, Lee G, Kim DH et al. Linearly and highly pressure-sensitive electronic skin based on a bioinspired hierarchical structural array. *Adv Mater* **28**, 5300–5306 (2016).
24. Liu L, Huang Y, Li FY, Ma Y, Li WB et al. Spider-web inspired multi-resolution graphene tactile sensor. *Chem Commun* **54**, 4810–4813 (2018).
25. Tung TT, Robert C, Castro M, Feller JF, Kim TY et al. Enhancing the sensitivity of graphene/polyurethane nanocomposite flexible piezo-resistive pressure sensors with magnetite nanospacers. *Carbon* **108**, 450–460 (2016).
26. Yue Y, Liu NS, Liu WJ, Li M, Ma YA et al. 3D hybrid porous Mxene-sponge network and its application in piezoresistive sensor. *Nano Energy* **50**, 79–87 (2018).
27. Gao YY, Yan C, Huang HC, Yang T, Tian G et al. Microchannel-confined mxene based flexible piezoresistive multifunctional micro-force sensor. *Adv Funct Mater* **30**, 1909603 (2020).
28. Pang Y, Zhang KN, Yang Z, Jiang S, Ju ZY et al. Epidermis microstructure inspired graphene pressure sensor with random distributed spinosum for high sensitivity and large linearity. *ACS Nano* **12**, 2346–2354 (2018).
29. Nie P, Wang RR, Xu XJ, Cheng Y, Wang X et al. High-performance piezoresistive electronic skin with bionic hierarchical microstructure and microcracks. *ACS Appl Mater Interfaces* **9**, 14911–14919 (2017).
30. Wang J, Tenjimbayashi M, Tokura Y, Park JY, Kawase K et al. Bionic fish-scale surface structures fabricated via air/water interface for flexible and ultrasensitive pressure sensors. *ACS Appl Mater Interfaces* **10**, 30689–30697 (2018).
31. Chang TH, Tian Y, Li CS, Gu XY, Li KR et al. Stretchable graphene pressure sensors with shar-pei-like hierarchical wrinkles for collision-aware surgical robotics. *ACS Appl Mater Interfaces* **11**, 10226–10236 (2019).
32. Xia KL, Wang CY, Jian MQ, Wang Q, Zhang YY. CVD growth of fingerprint-like patterned 3D graphene film for an ultrasensitive pressure sensor. *Nano Res* **11**, 1124–1134 (2018).
33. Zhou W, Ling WS, Liu W, Peng YJ, Peng JH. Laser direct micromilling of copper-based bioelectrode with surface microstructure array. *Opt Laser Eng* **73**, 7–15 (2015).
34. Gao Y, Li Q, Wu RY, Sha J, Lu YF et al. Laser direct writing of ultrahigh sensitive SiC-based strain sensor arrays on elastomer toward electronic skins. *Adv Funct Mater* **29**, 1806786 (2019).
35. Xin YY, Zhou J, Xu XZ, Lubineau G. Laser-engraved carbon nanotube paper for instilling high sensitivity, high stretchability, and high linearity in strain sensors. *Nanoscale* **9**, 10897–10905 (2017).
36. Huang KY, Ning HM, Hu N, Liu F, Wu XP et al. Ultrasensitive MWCNT/PDMS composite strain sensor fabricated by laser ablation process. *Compos Sci Technol* **192**, 108105 (2020).
37. Lu C, Gao Y, Yu GH, Xu MD, Tan JP et al. Laser-microengineered flexible electrodes with enhanced sensitivity for wearable pressure sensors. *Sens Actuators A Phys* **281**, 124–129 (2018).
38. Liu W, Xu FJ, Zhu NH, Wang S. Mechanical and electrical properties of carbon nanotube/polydimethylsiloxane composites yarn. *J Eng Fiber Fabr* **11**, 36–42 (2016).
39. Romoli L, Fischer F, Kling R. A study on UV laser drilling of PEEK reinforced with carbon fibers. *Opt Laser Eng* **50**, 449–457 (2012).
40. Zhang DS, Sugioka K. Hierarchical microstructures with high spatial frequency laser induced periodic surface structures possessing different orientations created by femtosecond laser ablation of silicon in liquids. *Opto-Electron Adv* **2**, 190002 (2019).
41. Wang ZY, Guan X, Huang HY, Wang HF, Lin WE et al. Full 3D printing of stretchable piezoresistive sensor with hierarchical porosity and multimodulus architecture. *Adv Funct Mater* **29**, 1807569 (2019).
42. Liu WJ, Liu NS, Yue Y, Rao JY, Cheng F et al. Piezoresistive pressure sensor based on synergistical innerconnect polyvinyl alcohol nanowires/wrinkled graphene film. *Small* **14**, 1704149 (2018).
43. Luo YH, Wu DZ, Zhao Y, Chen QN, Xie Y et al. Direct write of a flexible high-sensitivity pressure sensor with fast response for electronic skins. *Org Electron* **67**, 10–18 (2019).
44. Nichols WW. Clinical measurement of arterial stiffness obtained from noninvasive pressure waveforms. *Am J Hypertens* **18**, 3–10 (2005).
45. Zhang L, Pan J, Zhang Z, Wu H, Yao N et al. Ultrasensitive skin-like wearable optical sensors based on glass micro/nanofibers. *Opto-Electron Adv* **3**, 190022 (2020).

Acknowledgements

This work was supported by the National Natural Science Foundation of China (No. 51922092 and No. 51705439), Domain Foundation of Equipment Advance Research of 13th Five-year Plan (JZX7Y20190243000801), the Natural Science Foundation of Fujian Province of China (No. 2017J06015), and Science and Technology Plan Project of Xiamen City (No. 3502Z20173024). In addition, Fundamental Research Funds for the Central Universities (No. 20720200068) are also acknowledged.

Author contributions

C. Y. Zhang proposed the original idea and carried out most works. W. Zhou supervised the project. D. Geng, C. Bai and W. D. Li contributed in sample fabrication and measurements. S. Y. Chen contributed in revision of this paper. L. F. Qin and Y. Xie provided help in signal analysis.

Competing interests

The authors declare no competing financial interests.

Ethical statement

The tests related to human activities were performed with the help of C. Y. Zhang. All the experiments were carried out with his full and informed consent. Our experiments were only limited to surface contact between the sensor and skin, which does no harm to human participants.

Supplementary information

Supplementary information for this paper is available at https://doi.org/10.29026/oea.2021.200061